Monthly Notices
of the
ROYAL ASTRONOMICAL SOCIETY

Mon. Not. R. Astron. Soc. **416,** 465–478 (2011) doi:10.1111/j.1365-2966.2011.19056.x

Mercer 5: a probable new globular cluster in the Galactic bulge

A. J. Longmore,[1⋆] R. Kurtev,[2] P. W. Lucas,[3] D. Froebrich,[4] R. de Grijs,[5] V. D. Ivanov,[6] T. J. Maccarone,[7] J. Borissova[2] and L. M. Ker[8]

[1]*UK Astronomy Technology Centre, Royal Observatory, Blackford Hill, Edinburgh EH9 3HJ*
[2]*Departamento de Física y Astronomía, Facultad de Ciencias, Universidad de Valparaíso, Av. Gran Bretaña 1111, Playa Ancha, Casilla 5030, Valparaíso, Chile*
[3]*Centre for Astrophysics Research, University of Hertfordshire, College Lane, Hatfield AL10 9AB*
[4]*Centre for Astrophysics and Planetary Science, University of Kent, Canterbury CT2 7NH*
[5]*Kavli Institute for Astronomy and Astrophysics, Peking University, Yi He Yuan Lu 5, Hai Dian District, Beijing 100871, China*
[6]*European Southern Observatory, Ave. Alonso de Cordova 3107, Casilla 19, Santiago 19001, Chile*
[7]*School of Physics and Astronomy, University of Southampton, Hampshire SO17 1BJ*
[8]*Institute for Astronomy, Royal Observatory, Blackford Hill, Edinburgh EH9 3HJ*

Accepted 2011 May 11. Received 2011 May 11; in original form 2010 August 27

ABSTRACT

We present a detailed study of a dust-obscured Galactic star cluster Mercer 5 ([MCM2005b] 5) in an extremely crowded field in the Milky Way. Near-infrared (near-IR) photometry from United Kingdom Infrared Digital Sky Surveys (UKIDSS) and the Son of ISAAC on the New Technology Telescope (SofI/NTT), combined with near-IR spectroscopy also from SofI, indicates that it is almost certainly a Galactic globular cluster, located at the edge of the Galactic bulge. The cluster suffers ∼9 mag of visual extinction, with strong evidence for an extinction gradient across the cluster. A simulation of the differential reddening in the cluster using empirical data from NGC 6539 (chosen because it had high signal-to-noise ratio data and low field star contamination) as a template mimics the observations extremely well. This simulation and other arguments are used to indicate that the most prominent clump of stars in the colour–magnitude diagrams is a horizontal branch clump. On this basis we conclude that the cluster is at a distance of ∼5.5 kpc and suffers from visual extinction ranging from ∼8.5 to ∼12.5 mag. Alternative explanations for its nature, such as a young cluster or an old open cluster, are much less likely, on the grounds of no visible main sequence or stars with IR excesses for the former and location versus lifetime arguments for the latter.

Key words: stars: abundances – stars: distances – Galaxy: abundances – globular clusters: general – globular clusters: individual: Mercer 5: [MCM2005b] 5.

1 INTRODUCTION

One of the main general outcomes of new wide-field surveys is a statistically significant increase in the number of catalogued, classified objects, whether galaxies, stars, dark clouds or galaxy or star clusters. In the star cluster regime this has certainly been true for the Two Micron All Sky Survey (2MASS; e.g. Dutra & Bica 2001; Ivanov et al. 2002; Froebrich et al. 2007b; Ivanov et al. 2010) and *Spitzer* GLIMPSE surveys (e.g. Benjamin et al. 2003; Mercer et al. 2005). It will undoubtedly be so too for the United Kingdom Infrared Digital Sky Surveys (UKIDSS; Lawrence et al. 2007) and indeed some initial lists of, for example, new brown dwarfs (Burningham et al. 2010) are already becoming available. Because of its excellent depth and good angular resolution, the UKIDSS Galactic Plane Survey (GPS; see Lucas et al. 2008) is resulting in the discovery of many new Galactic clusters, mostly ones that have previously remained undetected because of dust obscuration (Lucas et al. 2009). Also, a lot can be learned by re-examining in the UKIDSS data clusters recently identified through other infrared (IR) surveys, notably 2MASS and GLIMPSE. Mercer et al. (2005) list 92 new star clusters. 25 of these are potentially in the area surveyed by GPS and all of them are now within the coverage of the latest (DR7) GPS release, in each of the J, H and K wavebands. One (Mercer 17) is only partially covered spatially. In this paper we examine in detail one of these clusters (Mercer 5). This cluster was chosen for such follow-up because it illustrates well the challenges of analysis of crowded stellar fields and because simple inspection did not lead to a clear identification of the nature of the cluster. The vast majority of newly discovered, hidden clusters appear to be a few million years old (Ivanov et al. 2002, 2005a; Borissova et al. 2003, 2005, 2006; Kurtev et al. 2007; Messineo et al. 2009, 2010) but a few have proved to be analogues of 'classical' globular clusters (Hurt et al. 2000, GC01 & GC02; Ortolani, Bica & Barbuy 2000, ESO 280-SC06; Carraro 2005, Whiting 1; Froebrich, Meusinger

⋆E-mail: andy.longmore@stfc.ac.uk

& Scholz 2007a, FSR 1735). There are probably still some 'missing' globulars in the central region of the Milky Way, based on the asymmetry argument of the GC distribution (Ivanov, Kurtev & Borissova 2005b) and/or more generally on the fact that they are still being discovered, albeit in very small numbers. Indeed the new ESO IR large survey 'VVV Vista Variables in Via Lactea' (Minniti et al. 2010) has already discovered a new low-mass globular cluster, VVV CL001, in the direction of the galactic bulge (Minniti el al. 2011).

Mercer 5, located well within the direction of the Galactic bulge and very close to the Galactic plane, is listed in Mercer et al. (2005) as a star cluster at position $l = 17\overset{\circ}{.}594, b = -0\overset{\circ}{.}110$ [RA (J2000) $\alpha = 18^{\rm h}23^{\rm m}19^{\rm s}$ and Dec. (J2000) $\delta = -13^\circ40'02''$], with radius 0.6 arcmin and an estimated 114 members. They also identified the cluster in 2MASS data, using the same search algorithm. A visual estimate of the cluster centre from the UKIDSS K-band image gave coordinates of $\alpha = 18^{\rm h}23^{\rm m}19\overset{\rm s}{.}8$, $\delta = -13^\circ40'07''$ ($l = 17\overset{\circ}{.}594; b = -0\overset{\circ}{.}112$), or approximately 12 arcsec east and 5 arcsec south of the Mercer et al. (2005) position. We compare near-IR photometry (J-, H- and K-band) results directly taken from the UKIDSS GPS catalogue with point spread function (PSF) photometry of the same data, additional near-IR photometry and spectroscopy from the Son of ISAAC on the New Technology Telescope (SofI/NTT; Moorwood, Cuby & Lidman 1998). In Section 5 we derive cluster properties such as distance and reddening, and, drawing on the near-IR spectroscopy results as indicative of cluster metallicity, compare these with isochrones covering a range of cluster ages.

2 OBSERVATIONS

2.1 Mercer 5: a new globular cluster candidate

Mercer 5 ([MCM2005b] 5) is a small, centrally condensed red star cluster that was also detected independently by one of us (PWL) during visual inspection of the UKIDSS pre-release data. Early clues suggested that it could be a promising candidate for a new Galactic globular cluster, due first to its position in the galaxy – in or close to the edge of the Galactic bulge, where many known globular clusters are found (e.g. Barbuy et al. 1998; Ortolani et al. 2010) – and secondly to its visual appearance in deep K-band images as a centrally condensed star cluster. A new Galactic globular cluster constitutes an exciting find, as the number of known Milky Way globular clusters has increased only by a few per cent over the last 20 years (e.g. Froebrich et al. 2007a). Specific examples include those already mentioned in Section 1. In addition, Ortolani et al. (2009) recently identified the cluster Pfleiderer 2 (Pfleiderer et al. 1977) as a globular cluster; Strader & Kobulnicky (2008) studied Mercer 3 ([MCM2005b] 3) and concluded that it was probably a globular cluster suffering an extinction $A_V \sim 24$ mag; the same conclusion for the same cluster, but under the name GLIMPSE-CO2, was reached by Kurtev et al. (2008), who showed that it is a metal-rich globular, suffering 24.8 mag of extinction.

For Mercer 5, in addition to the archived aperture photometry catalogue J-, H- and K-band pixel data were also downloaded from the Wide Field Camera (WFCAM) science archive (WSA, Hambly et al. 2008). Three images were obtained in the form of multiframes, with multiframe identifications from DR3 of 1452163, 1450228 and 1450876 for the J-, H- and K-band images, respectively, each having 0.2 arcsec pixel sizes. A 1000×1000 pixel^2 area was extracted, since this was adequate to encompass the whole extent of the cluster, with a sufficient area of background for later analysis. This resulted in a field of approximately 3.3×3.3 arcmin^2.

2.1.1 UKIDSS data: aperture photometry

Only aperture photometry is automatically carried out by the WFCAM pipeline, although overlapping apertures are simultaneously fitted, and the fluxes in overlap areas apportioned to each source according to the total flux, so photometry of a quality comparable to PSF photometry should be produced for most fields. Initially, the aperture photometry from the Data Release 4 (DR4) archive data was used for a preliminary examination of the cluster. Colour–colour ($J-H, H-K$) and colour–magnitude ($K, J-K$ and $K, H-K$) diagrams were plotted for the 3.3×3.3 arcmin^2 area described above. Visual inspection of the plots, including highlighting stars within 0.6 and 0.4 arcmin of the cluster nominal centre and combining these with 2MASS data for the brightest stars (see below) gave some indication that the cluster may indeed be a globular cluster. Comparison with background regions of the same area showed that a concentration of stars in the colour–magnitude diagram (CMD) around $K = 13.3, H-K = 0.7$ could be either a horizontal branch (HB) red clump or red giant branch (RGB) bump at a magnitude fairly consistent with the brightest stars being on the tip of the RGB of a cluster (see Section 5).

2.1.2 UKIDSS data: PSF fitting photometry

Although recent tests have shown no significant gain in precision by PSF fitting for most fields (see Lucas et al. 2008), as can be seen from Fig. 1, the Mercer 5 field is so crowded that we decided to perform PSF photometry to compare with aperture photometry, using the DAOPHOT II package, bundled in IRAF (Stetson, Davis & Crabtree 1990; Davis 1994). The PSF photometry detected about twice as many sources at each wavelength than the aperture photometry (Table 1). The J, H and K PSF photometry catalogues were then matched within Starlink's TOPCAT application (see http://www.starlink.rl.ac.uk/Bulletin/bulletin23.pdf) using a 0.5-arcsec separation criterion, using the triple match facility inclusive of all data, i.e. a final catalogue of all matched and

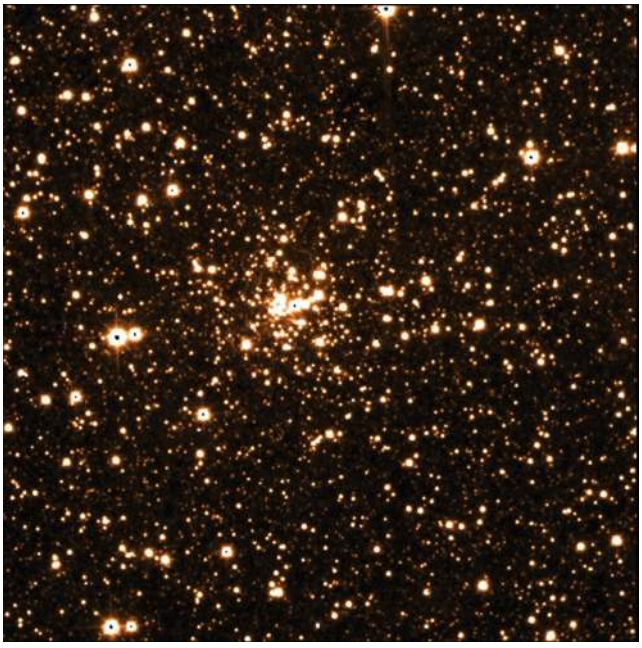

Figure 1. Mercer 5 K-band 3.3×3.3 arcmin^2 image from UKIDSS GPS survey.

Table 1. Number of detected stars at each wavelength for the UKIDSS GPS aperture photometry and the PSF photometry of the same images.

Catalogue	Aperture detections	DAOPHOT detections
J	2246	4619
H	3374	7055
K	3868	7303

Table 2. Completeness measurements for DAOPHOT photometry. The last column, *K* (CL), shows the completeness factor for radius $r < 0.6$ arcmin.

Magnitude (bin size = 0.5 mag)	Completeness factor			
	J	*H*	*K*	*K* (CL)
12.25	0.53	0.44	0.88	
12.75	0.99	0.97	0.95	
13.25	0.99	1.00	0.99	0.87
13.75	0.99	0.99	0.98	0.83
14.25	1.00	1.00	0.98	0.68
14.75	0.98	0.99	1.00	0.73
15.25	0.98	0.98	0.98	0.56
15.75	0.99	0.98	0.96	0.40
16.25	0.99	0.97	0.96	0.30
16.75	1.00	0.99	0.96	0.08
17.25	0.98	0.95	0.95	0.00
17.75	0.98	0.95	0.92	
18.25	0.97	0.90	0.88	
18.75	0.95	0.67	0.61	

unmatched detections for the three bands was produced. Finally, these were calibrated to the WFCAM system by direct comparison with the UKIDSS catalogue data.

For the PSF photometry sources containing saturated pixels (>39 000 counts) were rejected. This results in many bright stars included in the archive catalogue being absent from the PSF photometry catalogue. The effect of this can be seen in the completeness tests described for Table 2. Despite this, about twice as many stars were detected at all wavelengths using the PSF photometry as were found in the archive.

2.1.3 *Completeness tests*

Completeness tests were carried out in order to better understand the effects of crowding on results, by the usual technique of adding artificial stars to the frame using the ADDSTAR facility in DAOPHOT (Stetson 1996) and measuring the recovered fraction, using the same PSF as deduced for the original photometry. Repeats of this process were carried out in the *K* band only, over a smaller magnitude range, to determine the completeness within 0.6 arcmin of the cluster centre and investigate the effect of the extra crowding in the cluster region. Results are shown in Table 2. The *H* band has the highest average background count level across the frame, leading to a relatively quick onset of saturation in magnitude terms (only 44 per cent complete for stars with $12 < H \leq 12.5$). It would be the sample-limiting passband at the bright end if we were to use only UKIDSS data for the study.

2.1.4 *SofI data: PSF photometry and spectroscopy*

Independently, new near-IR photometry and spectroscopy of Mercer 5 had been carried out by one of us (RK). All observations were obtained with SofI/NTT on 2006 April 15. The instrument was equipped with a Hawaii HgCdTe 1024 × 1024 pixel^2 detector, with a pixel scale of 0.288 arcsec pixel^{-1}. For the spectroscopy we used a 1-arcsec slit and the medium-resolution grism, yielding a resolution of $R \sim 1320$ at 2.2 μm. The seeing for all observations was 1–1.5 arcsec and the sky was photometric.

We collected a total of 16-min integration in each of the *J*, *H* and *K* filters, split into 16 images, jittering within a 3-arcmin square box to ensure that there is minimum overlapping of the cluster position. Each individual image was the average of 3 × 20 s frames in *J*, 6 × 10 s frames in *H* and 10 × 6 s frames in *K*. The data reduction included flat-fielding, sky subtraction, alignment and combination of the individual images. The stellar photometry was carried out on the final images with ALLSTAR in DAOPHOT II (Stetson 1996). The typical SofI photometric errors range from 0.01 mag for stars with $K \sim 10$ to 0.10 for $K \sim 18$ and 0.15 for $K \sim 19$. The photometric calibration was performed by comparing our SofI instrumental magnitudes with the UKIDSS catalogue measurements of about 2500 stars, covering the magnitude range of about $12 \leq J, H, K \leq 16$ and a wide range of colours. After calibration, the SofI–UKIDSS PSF magnitudes show excellent agreement at *H* and *K*, good agreement at $J = 13$, but a small offset of up to 0.04 mag brighter than this, justifying the use of SofI data at magnitudes brighter than 13. The final SofI photometry list contains equatorial coordinates and *J*, *H*, *K* magnitudes of 13 896 stars. Amongst them, 4762 stars have photometric errors less than 0.15 in *J*, *H* and *K*. Artificial star tests show that the 80 per cent completeness limit (CL) of the SofI photometry is at $J = 18.5$ and $K = 17.1$.

The spectra cover the ∼2.00–2.35 μm region. The telescope was nodded along the slit between the exposures to observe simultaneously the targets and clear sky. In total, we obtained eight images of 300 s. First, we flat-fielded them and removed the sky emission by subtracting from each field the images from each nodding pair. Next, we extracted one-dimensional spectra with the IRAF[1] task APALL, wavelength calibrated them with the NeXe lamp spectra (extracted at the location of the science target spectra), and combined them into final one-dimensional spectra. Finally, we divided them by the spectra we took from the solar near-analogue HIP 59642 (HD106290) of type G1V, and multiplied them by a solar spectrum to remove the artificial emission lines caused by the intrinsic absorption features in the spectra of the standard (see Maiolino, Rieke & Rieke 1996).

2.1.5 *Metal abundance from spectroscopy*

We derived the metal abundance of the cluster from the spectra of five cluster red giants (listed in Table 3), applying the method of Frogel et al. (2001), which is based on the behaviour of the *K*-band spectral indices, IR magnitudes and colours. The individual reddening and true colour of each star are obtained by moving the star along the reddening vector until it crosses the luminosity class III sequence taken from Frogel et al. (1978). All these stars are located near the cluster centre, and lie near the cluster RGB,

[1] IRAF is distributed by the National Optical Astronomy Observatory, which is operated by the Association of Universities for Research in Astronomy, Inc., under cooperative agreement with the National Science Foundation (NSF).

Table 3. Stars for which near-IR spectroscopy was obtained. Magnitudes given in italics indicate they are long-exposure SofI images, otherwise they are from short exposures.

No.	RA (°)	Dec. (°)	*J*	*H*	*K*
1	275.831 62	−13.668 54	11.28	9.34	8.42
2	275.830 56	−13.668 78	13.54	11.43	10.50
3	275.830 02	−13.669 02	*14.85*	12.75	11.75
4	275.829 50	−13.669 43	12.11	9.93	*8.91*
5	275.832 96	−13.667 93	*13.72*	*12.16*	*11.44*

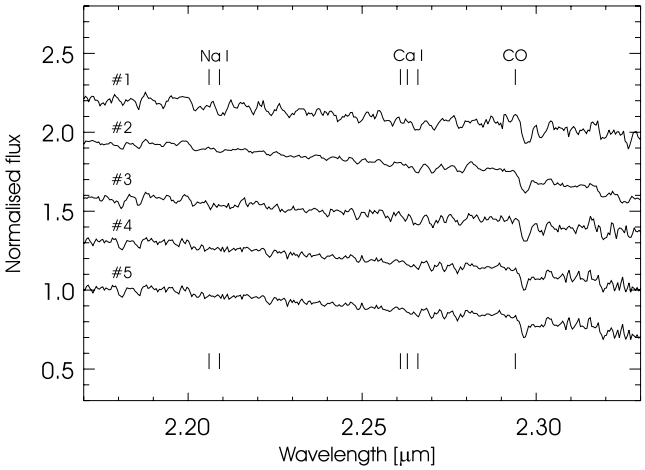

Figure 2. *K*-band spectra of the five probable cluster red giants listed in Table 3. The position of the Na doublet, the Ca triplet and the first CO bandhead are indicated.

making them probable members, although star #1 differs from the other four and could be a field star.

The spectra are plotted in Fig. 2. We were only able to measure reliably the equivalent widths of the CO 2.3-μm feature, and applied the calibration (equation 4 of Frogel et al. 2001) that takes into account also the stellar colour $(J - K)_0$ and absolute magnitude M_K. Results are listed Table 4.

The table contains the equivalent widths of the CO lines, the deduced CO index based on the formula in Stephens & Frogel (2004), true colour $(J_s - K_s)_0$, estimated *K*-magnitude extinction A_K, absolute *K* magnitude M_K and metallicity on the scale of Zinn (as implemented in Harris 1996). In the calculation of the absolute magnitude, we used a value of $(m - M)_0 \sim 13.6$ for the distance modulus of the cluster. It is clear that the metal lines of Na I and Ca I were not sufficiently strong to measure at the acquired signal-to-noise ratio (S/N).

Table 4. Spectroscopic measurements of red giant stars in Mercer 5.

No.	EW CO	Index CO	$(J_s - K_s)_0$ (mag)	A_K (mag)	*K* (mag)	M_K (mag)	[Fe/H] from CO
1	9.93	0.08	0.89	1.31	8.42	−6.49	−0.89
2	6.75	0.04	0.71	1.54	10.50	−4.64	−1.41
3	6.91	0.04	0.68	1.57	11.78	−3.39	−1.38
4	6.83	0.04	0.87	1.54	8.91	−6.22	−1.40
5	7.16	0.05	0.77	1.50	11.44	−3.66	−1.34
				Mean (all)			−1.28 ± 0.10
				Mean (2–5)			−1.38 ± 0.04

Averaging the five estimates from the spectroscopy we obtain [Fe/H] = −1.28 ± 0.10 dex; ignoring star 1 the mean is −1.38 ± 0.04 dex. Three other stars for which spectra were obtained were not suitable for metallicity measurements, either because they were too faint or because they were early-type field stars. The error value given is the standard error of the mean of the formal [Fe/H] values, and does not include any systematic effects resulting from calculations of reddening or assumptions about the stellar temperatures. Given the high reddening values and the overall observational difficulties of working in such crowded fields, we believe that the final error could be as high as ±0.4 dex.

Thus, importantly for later discussion, the cluster could just fall into the relatively metal-rich category of globular clusters with [Fe/H] ∼ −1 dex.

3 MERCER 5 RESULTS AND PRELIMINARY ANALYSIS

3.1 Simple King model χ^2 fits to cluster surface brightness profile

A surface brightness profile, or SBP, was constructed for the cluster assuming spherical symmetry. The *K*-band image was used for this because of its depth and its reduced sensitivity to extinction by dust, although some small unrecoverable error will exist because of image saturation effects. Aperture photometry was performed using the Starlink package GAIA (http://starlink.jach.hawaii.edu/docs/sun214.htx/sun214.html#xref_) in a series of annuli about the visually determined centre of the cluster. The derived surface brightness profile is shown in Fig. 3.

Both the star number radial density profile (RDP) and the surface brightness profile can be used to assess structural parameters for a cluster. The SBP can suffer from significant noise from varying background levels in the regions outside the cluster and also from random effects of relatively bright stars throughout the frame, whether field or cluster members. The RDP, based on number counts of stars, is generally accepted to be useful for the outer parts of a cluster if a reasonably uniform background field is available (see Bonatto et al. 2007). This is not true for Mercer 5, and the CLs are very poorly defined towards the centre of the cluster. The SBP is therefore used here to investigate structural parameters of the cluster.

We employed the often-used King (1966) model to fit the SBP. These are single-mass, modified isothermal sphere models which fit structural parameters core radius r_c and the tidal radius r_t, as well as background flux and peak (central) flux. The core radius is defined as the radius where the cluster SBP falls to half the central surface brightness.

In practice the King model gave poor χ^2 fits and the core radius solution depended significantly on the smallest radius r_{min} sampled, for example varying by a factor of ∼2 between $r_{min} = 18$ and 24 pixel. The key problem is in determining an appropriate background level. We eventually did this by iterating manually.

It is clear from Fig. 3(b) that it is possible to choose a background level that, within the noise, appears to give a flat profile outside ∼1 arcmin radius. Subtracting a significantly larger background/pixel causes a turnover in the total counts; a smaller background has the cluster increasing in total counts up to the limit of sensible radius measurement. Adopting 1 arcmin as the cluster radius therefore should be treated as a minimum value: it almost certainly extends beyond this (as discussed in Section 5.1), but no upper limit can be derived because of the large statistical fluctuations in the

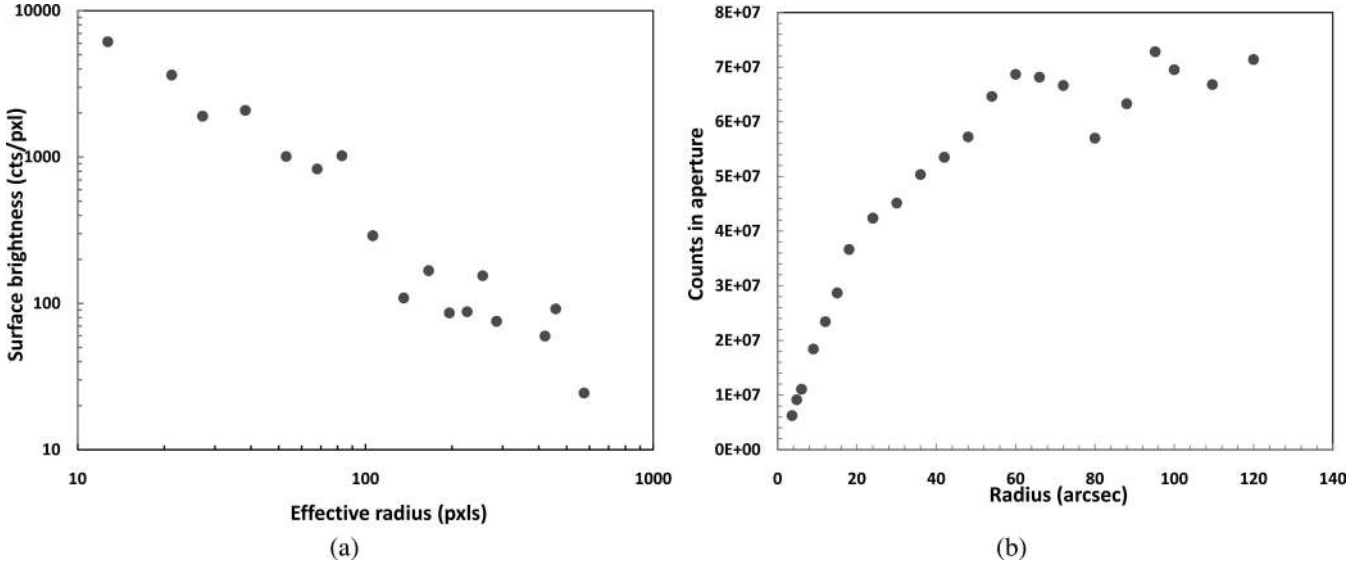

Figure 3. (a) Logarithmic surface brightness profile in mean count pixel^{-1} (1 pixel $\equiv$ 0.4 arcsec), centred on revised position of cluster. No background has been subtracted in this plot. (b) Total count versus radius, background subtracted with its value set to stabilize differential counts at >1 arcmin (see text).

background. On this basis, *minimum* half-light, 75 per cent light and 90 per cent light radii, were derived as $r_{0.5} = 17$ arcsec, $r_{0.75} = 36$ arcsec and $r_{0.9} = 47$ arcsec, respectively. We have adopted the Mercer value of $r < 36$ arcsec as our analysis area for the cluster stars, because the nominal 75 per cent radius includes a good proportion of cluster members while minimizing confusion by field stars in the CMDs and colour–colour diagram (CCDs).

Table 5. Magnitude range used to select stars for composite CCDs and CMDs.

K magnitude range	Source
$K \leq 13$	SofI short exposure
$K > 13$	UKIDSS

3.2 Preliminary examination of photometry

3.2.1 JHK colour–magnitude diagrams

K, $J - K$ and K, $H - K$ CMDs were constructed based on a combination of PSF photometry from the UKIDSS data and the SofI data over the adopted 3.3×3.3 arcmin^2 field and for a region of radius $r < 0.6$ arcmin centred on the cluster. Because of the short integration times and smaller pixel and telescope sizes used to obtain the SofI data, bright star detections in SofI are more complete and will be less affected by non-linearities. Because of the higher angular resolution, the SofI photometry is also more robust against contamination effects from crowding than 2MASS data in this region. However, even the SofI data saturated for the brightest stars, so we initially included the 2MASS data in the composite diagrams. When plotted in CCDs, the 2MASS stars lay well away ($\sim$0.2 mag) from any other giants in the diagram. For stars of $K \sim 8.5$ the maximum non-linearity in the SofI data is $\sim$5 per cent: with this caveat we chose to use only the SofI and UKIDSS data for our analysis. Only one additional star would have been included with the adopted cluster radius had we used the 2MASS data. For simplicity, magnitude boundaries to select which catalogue to use were based on the K band. Because the vast majority of sources are red the effects of saturation at shorter wavelengths will be minimal or absent. Magnitude boundaries used are shown in Table 5.

The main features in the $r < 0.6$ arcmin $K, J - K$ diagram (Fig. 4, left) appear at first to show a weak RGB with a lot of scatter, with the brightest RGB member likely to be in the range $K \sim 8$–9, and a putative clump of stars at $K \sim 13.32$, $J - K \sim 2.02$, $H - K \sim 0.60$ (hereafter clump 1). Such clumps in globular clusters are usually attributable to either a horizontal branch (HB) red clump, common in relatively high-metallicity globular clusters – for example see Valenti et al. (2005, 2007) and Kim et al. (2006) – or an RGB bump (ibid., Ferraro et al. 2006; Valenti et al. 2010). However, with such a high level of field (background + foreground) contamination, the giant branch is very poorly defined and the nature of this clump as either an RGB bump or an HB red clump is not readily discernable. Statistically, the evidence for the presence of a cluster RGB is reasonable: for example, in Fig. 4 there are 17 stars in a region $K < 11, 2.0 < J - K < 3.5$ where an RGB associated with the cluster bump/clump as described above might lie, but only four stars in a background region of the same area.

For comparison, the same plot is shown (Fig. 4, right) in an annulus having the same area and inner radius $r = 1.5$ arcmin. A weak concentration is seen at the same colour in the diagram as clump 1, possibly slightly brighter, and not as prominent as for the region centred on the cluster. The number of stars fainter than $K \sim 15$ in the background region is far higher than that within $r = 0.6$ arcmin, demonstrating the lower completeness factor in the cluster region. An additional feature in the cluster region is a comparative excess of stars with $13.5 < K < 14.1, 2.4 < J - K < 3.0$. Similar behaviour is seen for the $K, H - K$ diagrams (Fig. 5). Detailed interpretation is given in Section 5.1.

Some authors attempt to correct for background statistically by computing the number of field stars expected in a particular magnitude and colour cell from background observations and subtracting the expected number of field stars from each cell (see e.g. Bonatto et al. 2007). However, since the number count of stars within the cluster is significantly affected by self-crowding, attempts to do this were not successful. In Section 5.1 we instead look at statistics of the number density in various regions of the CMD for different field locations.

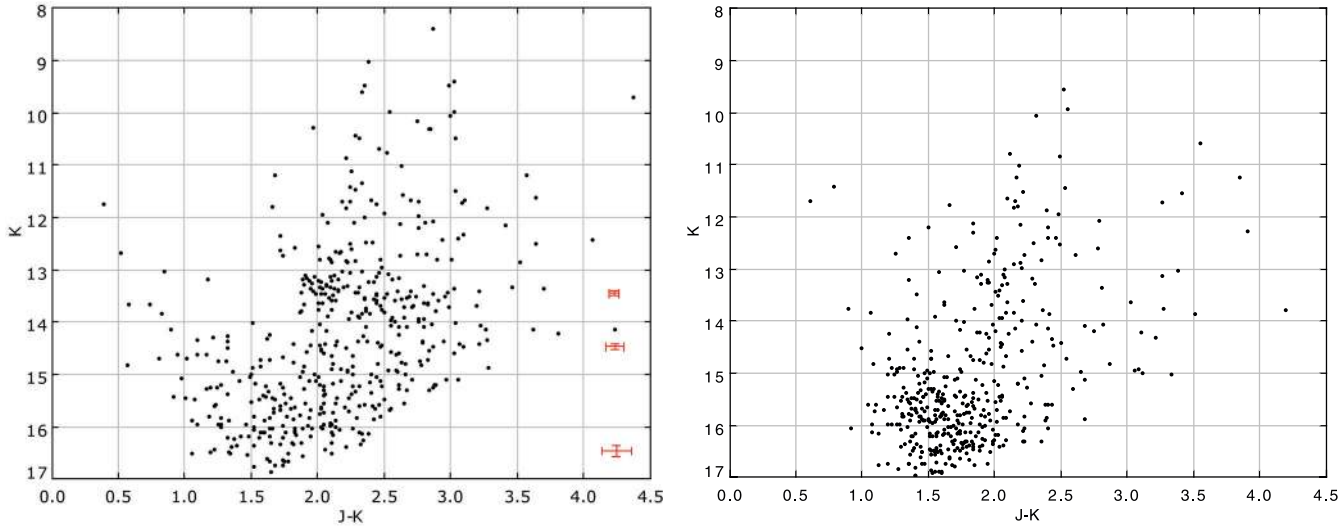

Figure 4. Left-hand panel: $K, J-K$ CMD with radius $r < 0.6$ arcmin from cluster centre (no background subtraction). Illustrative DAOPHOT error bars are shown for selected magnitudes. Right-hand panel: $K, J-K$ CMD of a background region with the same area as in the left-hand panel.

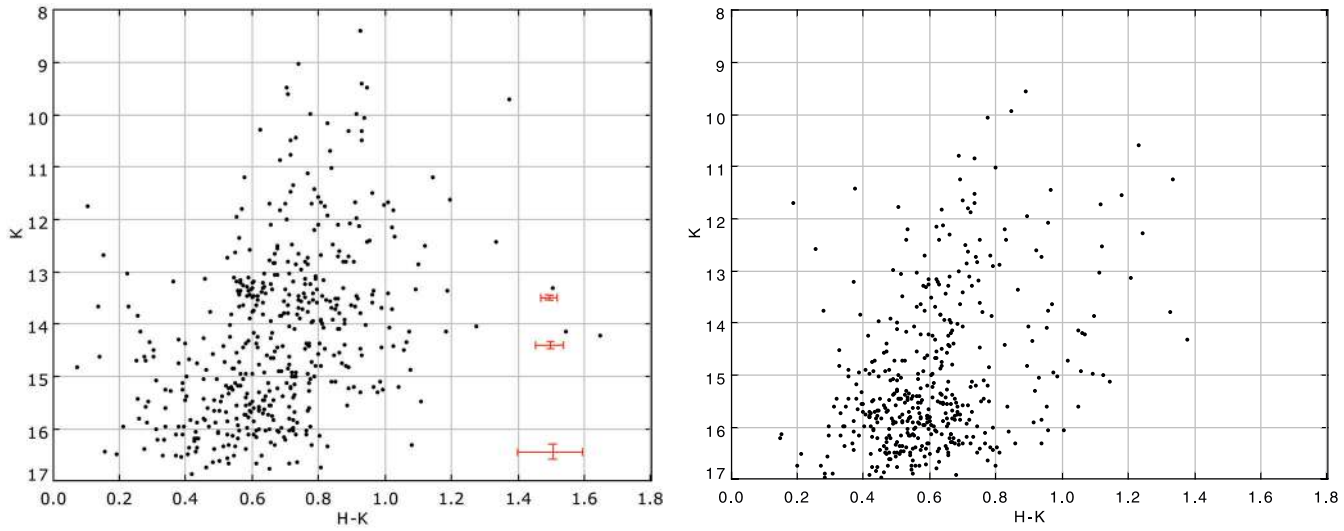

Figure 5. Left-hand panel: $K, H-K$ CMD of region within 0.6 arcmin of cluster centre (no background subtraction). Illustrative DAOPHOT error bars are shown for selected magnitudes. Right-hand panel: $K, H-K$ CMD of background annulus with the same area as in the left-hand panel.

3.2.2 $J-H, H-K$ CCD

The $J-H, H-K$ colour–colour diagrams for areas equivalent to those in Figs 4 and 5 are shown in Fig. 6. Inspection shows for the cluster region stars not only a much higher proportion of red stars but also an offset in locus towards a higher $J-H$ value for a given $H-K$. This is consistent with a higher fraction of more distant, giant stars both because of the presence of the cluster and the omission of faint nearby (dwarf) stars through crowding.

3.2.3 K-band luminosity function

To investigate the K-band luminosity function, or KLF, we combined the UKIDSS PSF photometry with that from SofI as described in Table 5. In Fig. 7, we show the KLF for all stars within a radius of 0.6 arcmin from the cluster centre, with photometric errors <7.5 per cent and with normalized background counts from the outer half of the frame subtracted.[2] The effect of the lower completeness fraction at fainter magnitudes is clearly seen in the negative counts at fainter magnitudes. Background-subtracted counts corrected for completeness are shown in Fig. 8. In both plots the excess of stars, with a bump in the luminosity function from magnitude 13 to 14, is obvious. The completeness correction for magnitudes fainter than $K \sim 16$ is sufficiently large that the numbers can be taken only as indicative that there should indeed be a rising luminosity function.

3.2.4 Mid-infrared properties – Spitzer GLIMPSE data

If Mercer 5 were a young open cluster rather than a globular cluster, it could show signs of recent star formation through stars with IR excesses. To test this, we constructed a $H-K$ versus [$K-$

[2] Only UKIDSS stars are included in the Fig. 8 histogram as these had uniform completeness correction determinations.

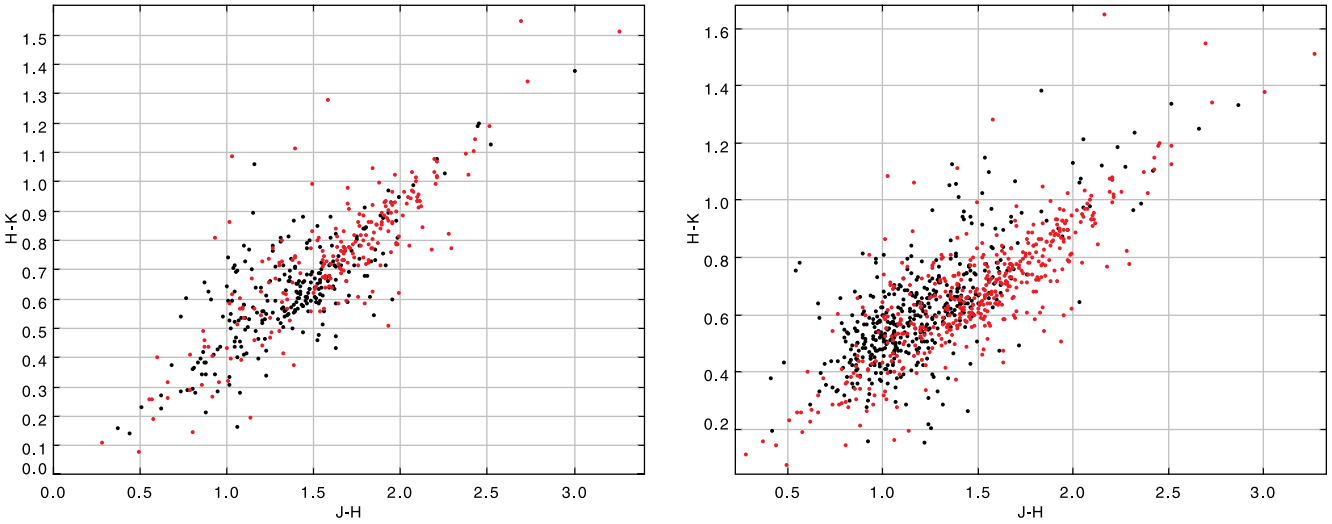

Figure 6. $J-H$, $H-K$ CCD. Left-hand panel: region within 0.6 arcmin of cluster centre; red symbols show stars south of centre, black symbols show stars north of centre (see Sections 3.2.2 and 5.1 for details). Right-hand panel: equal-area annulus with inner radius 1.5 arcmin, with the cluster region overplotted in red.

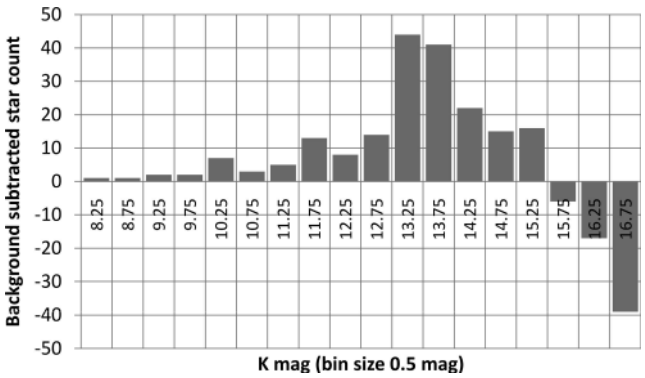

Figure 7. Histogram of star counts in the K band with average background subtracted, for a radius of 0.6 arcmin centred on the cluster. No completeness corrections are included. The 'negative' star counts at the faint end manifest the additional crowding-induced incompleteness within the cluster region.

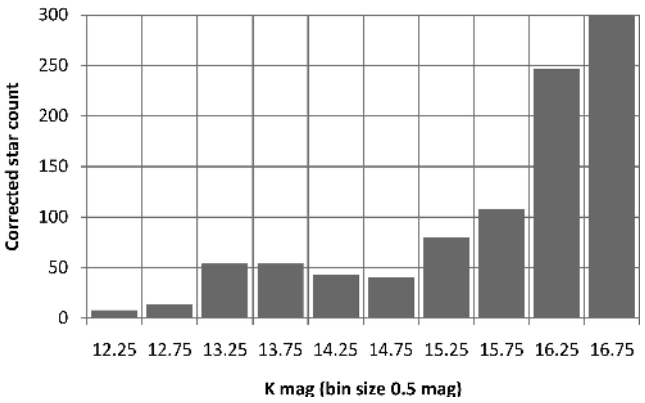

Figure 8. Histogram of star counts in the K band, corrected approximately for incompleteness. In order to show the luminosity bump in the 13–14 mag range, the bin centred on 16.75 is off scale, but has a value of 1114. Points at 12.25 and 12.75 mag assume 100 per cent completeness.

$m(4.5)$] CCD from a combined catalogue of SofI short-exposure and GLIMPSE photometry, limiting the selection to stars with GLIMPSE $m(4.5)$ errors of <0.1 mag. We found only three stars with significant IR excesses in $[K-m(4.5)]$. A background region with twice the total area had six stars with excesses using the same error criteria, so there is no evidence for an excess of very young objects in the region of the cluster.

4 CMD EXPECTATIONS FROM GALACTIC STRUCTURE

The field star density towards Mercer 5 is obviously extremely high. Before proceeding to further analysis of Mercer 5 itself, we therefore investigate expectations for CCDs and CMDs in its direction in the Galaxy. Robin (private communication) kindly supplied a plot of extinction versus distance out to 15 kpc in the direction of Mercer 5, calculated from the data described in Marshall et al. (2006) and this is applied to the Besançon model (Robin et al. 2003).

A giant branch sequence in the model, typical of those running diagonally across such an IR CMD above the locus of dwarf stars (e.g. Lucas et al. 2008), matches well at its bright limit an extended clump of stars in the UKIDSS GPS catalogue data, centred approximately at $K=13.0, J-K=2.1$. However, the giant sequence visible in the models does not extend faintwards very far in our observed data: any sequence is very weak below $K\sim14, J-K\sim2.3$, equivalent to distances beyond about 8 kpc. Most significantly, the PSF data in the area of the CMD where the cluster stands out most from the background (Fig. 4, left) show a sequence – approximately along a reddening vector – starting at about 0.25 mag fainter than the large-area giant sequence, but not appearing to be just a reddened version of this, because it extends further to the blue in the diagram than the background giant sequence. All features discussed above are reproduced also in the $K, H-K$ CMD. Even a model including a Galactic bar, run specially for us by Robin (private communication), did not show any overdensity in the CMDs like that in the cluster region (see Section 6 for more detail about this).

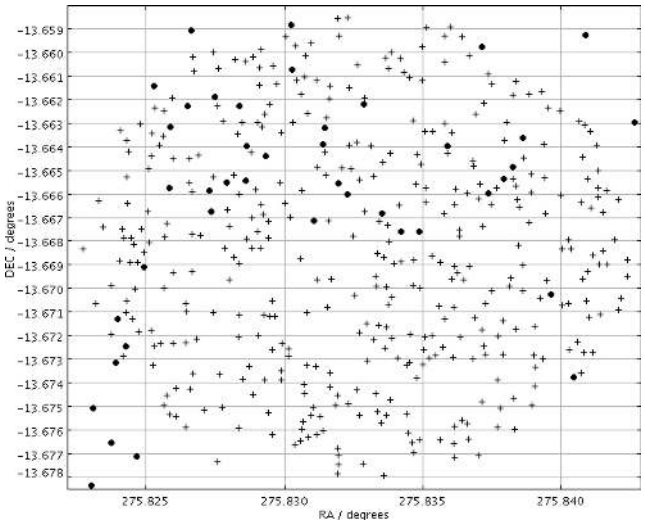

Figure 9. All stars with $H-K$ errors <7.5 per cent with $r < 0.6$ arcmin (crosses), overplotted with stars within clump 1 (circles).

5 MERCER 5 DETAILED ANALYSIS

5.1 (Differential) reddening

Guided by the apparent asymmetry of the cluster, we used the 'define subset' facility in TOPCAT to investigate the spatial location of the stars in clump 1, with the intriguing result found in Fig. 9.

For those stars in clump 1 (defined as $13.1 < K < 13.5, 0.5 < H - K < 0.7$ and shown as circles) that lie within 0.6 arcmin of the cluster centre, only five out of 28 lie in the southern half of the region, a 4.6×10^{-4} cumulative probability on a random basis. We therefore investigated the possibility that this was caused by dust extinction aligned approximately east–west across the centre of the cluster.

Fig. 10 shows the CMD for the same data as in Fig. 6 (left) but for sources in the north and south of the $r < 0.6$ arcmin region independently, with the boundary drawn at $\delta = -13^{\circ}40'07''$. The northern region appears to define a narrower RGB and has a better defined clump than the full region while the southern half shows a

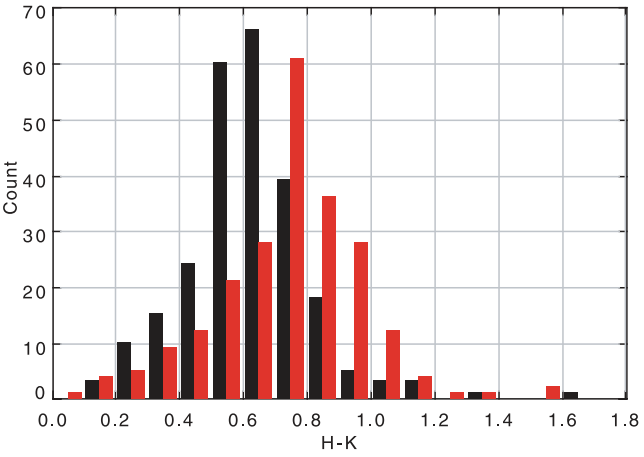

Figure 11. Histogram of $H-K$ star counts for $r < 0.6$ arcmin. Black: north half of region. Red: south half of region.

broader sequence that lies on average significantly redwards of the northern region, probably with elongation along a vector consistent with a range of additional reddening, as shown in the right-hand part of Fig. 10. This difference between the north and south areas can be seen clearly in Fig. 11, a histogram of the $H - K$ colour counts. The number counts follow a similar pattern, but with the southern set displaced ∼0.2 mag redwards. No significant asymmetry was found when a similar histogram was drawn with an east–west division.

It would seem that the scale of this differential reddening effect is confined locally to the region of the cluster, well within the borders of the 3.3 arcmin^2 field we studied in detail, since no obvious north/south asymmetry is seen on the larger scale. A possible cause of such an effect is discussed later in this section.

Meanwhile, we examine further the statistics of the CMD features. Table 6 shows number counts in the red clump region most clearly visible in the CMDs (region boundaries are given in the table heading).

It is immediately clear that the red clump has a highly significant excess number density centred on the cluster in both CMDs measured. In fact, the normalized number density of stars in this clump *outside* a given radius continues to fall even when the radius is set

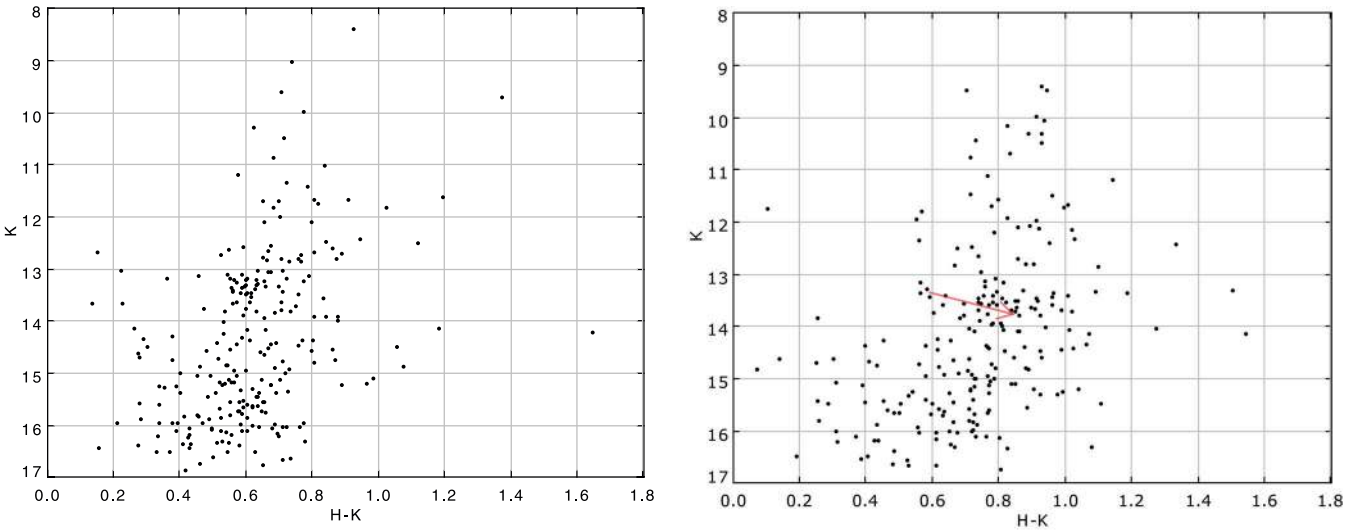

Figure 10. *K*, $H-K$ diagram of cluster, $r < 0.6$ arcmin. Left-hand panel: north of centre. Right-hand panel: south of centre, with reddening vector shown equivalent to $Av = 4$.

Table 6. Counts within a region of the CMD defined by $13.1 < K < 13.5$, and either $1.9 < J - K < 2.3$, or $0.55 < H - K < 0.7$.

Region relative to cluster (arcmin)	Normalized sky area[a] (deg^2)	Count $(K, J-K)$	Normalized count $(K, J-K)$	Count $(K, H-K)$	Normalized count $(K, H-K)$
$r < 0.6$	0.110	29	264	27	246
$r > 0.6$	1	118	118	107	107
$r < 0.6$, north	0.055	24	436	22	400
$r < 0.6$, south	0.055	5	91	5	91
$r < 1.0$	0.306	63	206	63	206
$r > 1.0$	0.804	84	104	71	88

[a]Sky area normalized to the region subject to DAOPHOT analysis excluding the region inside $r = 0.6$ arcmin.

Table 7. Counts within a region of the CMD defined by $13.4 < K < 13.85$, and either $2.3 < J - K < 2.75$, or $0.7 < H - K < 1.0$.

Region relative to cluster (arcmin)	Normalized sky area (deg^2)	Count $(K, J-K)$	Normalized count $(K, J-K)$	Count $(K, H-K)$	Normalized count $(K, H-K)$
$r < 0.6$	0.110	23	209	34	309
$r > 0.6$	1	36	36	70	70
$r < 0.6$ north	0.055	5	91	7	127
$r < 0.6$ south	0.055	18	327	27	491
$r < 1.0$	0.306	39	128	54	177
$r > 1.0$	0.804	20	25	50	62

to select half the total image area. This property, combined with the persistence, at a low level, of the red clump in the background areas with $1 < r < 1.5$ arcmin, and the overall number count growth curve in Fig. 3(a) shows that the cluster has clump members statistically detectable well outside the 36-arcsec core. Also, the difference between the northern and southern sky area inside $r = 0.6$ arcmin is confirmed in both CMDs, with a number density for the southern half not statistically significantly higher than the 'background' as defined by the density outside $r = 1$ arcmin.

This second point can be readily understood by carrying out a similar analysis on a CMD region approximately along a reddening vector from the red clump (Table 7). We learn from this table that in both CMDs there is another region of excess number density centred on the cluster, in the southern half of $r < 0.6$ arcmin, with a fairly similar (slightly lower) number density to that of the red clump in the northern part of the cluster.

The overall picture is therefore consistent with most of the cluster stars in the southern part of cluster within 0.6 arcmin that would have been seen in the red clump being reddened by additional extinction into a neighbouring region of the CMD. One might also expect an overdensity in other regions of the CMD that could be associated with a distant globular cluster: this is true for the giants in the CMD with $K < 12$ that might be expected to be seen as the cluster RGB, but there is no detectable excess at magnitudes significantly fainter than the red clump. In fact the number density within 0.6 arcmin is lower, consistent with a brighter limiting magnitude because of crowding, as discussed in Section 2.1.2.

Is there any additional evidence to support the differential reddening conclusion? This region is included in the Bolocam survey of the Galactic plane (Aguirre et al. 2011), mapping at 1.1 mm wavelength, sampled at 38-arcsec spacing with a nearly Gaussian beam of 31-arcsec FWHM. Fig. 12 shows a selected area ($\sim 30 \times 30$ arcmin^2) of the Bolocam density map centred on Mercer 5. The bright features, such as that aligned along declination $-13°50'$ near the bottom left of the image, coincide extremely well with high-extinction regions visible in UKIDSS. Although uncomfortably close to the apparent confusion limit (exacerbated by the fact that the original data are extracted from a chopped beam signal), there is some evidence for a dust feature located precisely across the southern half of Mercer 5. While by no means conclusive, it is at least consistent with differential reddening across the cluster. This is not unusual and is, in fact, often seen also across resolved extragalactic clusters; see e.g. Bastian et al. (2007) for M82-F and Cohen (2006) for the GC 037-B327 in M31.

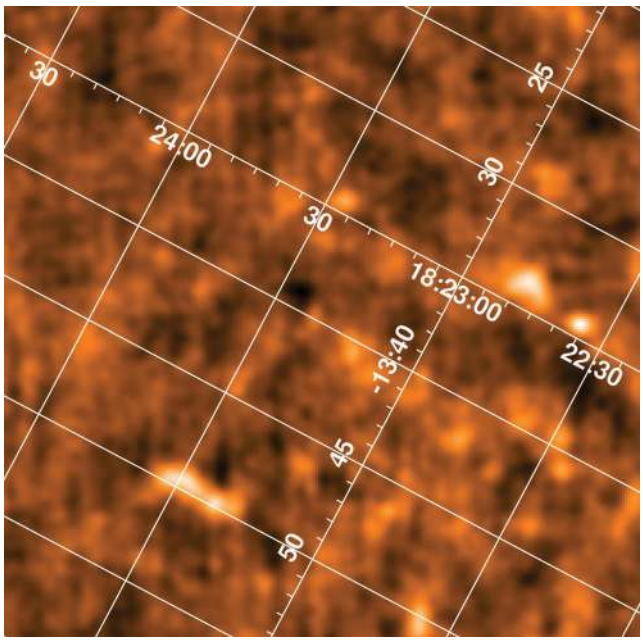

Figure 12. Bolocam density map centred on the position of Mercer 5.

5.2 Distance and reddening from empirical comparisons

We now seek to determine whether a consistent interpretation can be drawn of Mercer 5 as a globular cluster. The RGB reaches its maximum extent in luminosity for stellar populations older than 1–2 Gyr, when stars less massive than two solar masses are evolving, and remains approximately constant with the increasing age of the population (e.g. Valenti et al. 2004). At [Fe/H] $= -1.3$ dex there is $\sim$4.4 mag gap from the RGB bump to the RGB tip (Kim et al. 2006; Valenti et al. 2007), whereas the gap from HB clump to RGB tip is $\sim$5.1 mag. However, this latter value is deduced from the three most metal-poor clusters listed as having an HB clump, NGC 6380, 6638 and Ter 3, which between them have an average [Fe/H] ~ -0.9 dex. Ter 1, with [Fe/H] $= -1.1$ dex, also has a gap of 5.1 mag (Valenti et al. 2010). Figs 4 and 5 allow either possibility to apply to Mercer 5, with just one star making a difference of 0.75 mag in the possible gap.

We have analysed the CMDs' interpretations in terms of reddening and distance using a variety of optical–near-IR reddening laws, making minor adjustments as necessary for the UKIDSS filter wavelengths using a correction of the coefficients assuming a power-law wavelength dependence of absorption $A_\lambda \propto \lambda^{-1.8}$. Specifically, we have used results from studies by Rieke & Lebofsky (1985), the near-IR law from Cardelli et al. (1989), the mean value from He et al. (1995), Indebetouw et al. (2005), Stead & Hoare (2009), and a small selection of values from fits to different directions by Fitzpatrick & Massa (2009). Note that these cover a wide range in $R_V = A_V/E(B-V)$. The dominant factor in determining the distance to the cluster on any given interpretation of the clump is the ratio A_K/A_V in the reddening law, because K-band magnitude is used to calculate the distance modulus. For the laws investigated, these values had the range $0.07 \leq A_K/A_V \leq 0.118$, with both the extremes coming from examples in Fitzpatrick & Massa (2009). The resulting distance moduli ranged over 0.4 mag for a given clump interpretation. Comparing A_V results calculated from $E(J-K)$ and $E(H-K)$, the different laws gave a wide range of values for A_V and A_K, ranging over 1.7 and 0.4 mag, respectively, within a given filter combination. $E(J-K)$ invariably gave a higher value of A_V than did $E(H-K)$, by up to 1.4 mag. For the final calculations and diagrams we have adopted the law from Indebetouw et al. (2005). In calculations based on $J-K$, the more reliable baseline, these gave a result similar to that of Cardelli et al. (1989), Rieke & Lebofsky (1985) and He et al. (1995), but gave more consistent agreement between $J-K$ and $H-K$. The actual extinction coefficients used were $A_J/A_V = 0.282$, $A_H/A_V = 0.172$ and $A_K/A_V = 0.110$. Results are summarized in Table 8.

Without these additional uncertainties, but allowing for the uncertainty in the position of the observed clump, we estimate errors on the derived parameters as $\pm$ 0.25 mag for A_V derived from $E(J-K)$, $\pm$0.5 mag for A_V derived from $E(H-K)$ and $\pm$0.15 mag for $(m-M)_0$. However, actual values of A_V could be well outside these limits simply because of the uncertainty in the reddening law.

5.3 Isochrone comparisons

Using the mean metallicity derived from the spectroscopy, an estimate for the distance and reddening to the cluster was sought, through isochrone fitting by visual inspection. Various libraries of theoretical isochrones are available: we used the Padova data base of theoretical isochrones in the UKIDSS photometric system (available from http://stev.oapd.inaf.it/cgi-bin/cmd) with the Marigo et al. (2008) evolutionary tracks. As for the empirical comparisons, the best defined feature in both the K, $J-K$ and J, $H-K$ CMDs is the red clump in the northern half of the cluster. We fitted independently by eye the location of the red HB clump and then the RGB bump to isochrones of age 2, 4 and 10 Gyr, for metallicities of [Fe/H] $= -1.3$ and –0.9, with distance and reddening as the other variables. The scatter in the (weak) RGB is far greater than can be accounted for by photometric errors, almost certainly as a result of the differential reddening and field contamination, and means it helps little in constraining the isochrones. Similarly, the tip of the RGB is very poorly defined and provides no useful constraints, so the fits are entirely dominated by the properties of the clump.

Sample fits are shown in Fig. 13, plotted on K, $J-K$ and $J-H$, $H-K$ CMDs and CCDs of the $r < 0.6$ arcmin cluster region. Slightly different results are obtained depending on whether the $H-K$ or $J-K$ colour is used. The extinction law used was again that given by Indebetouw et al. (2005). The distance result is not

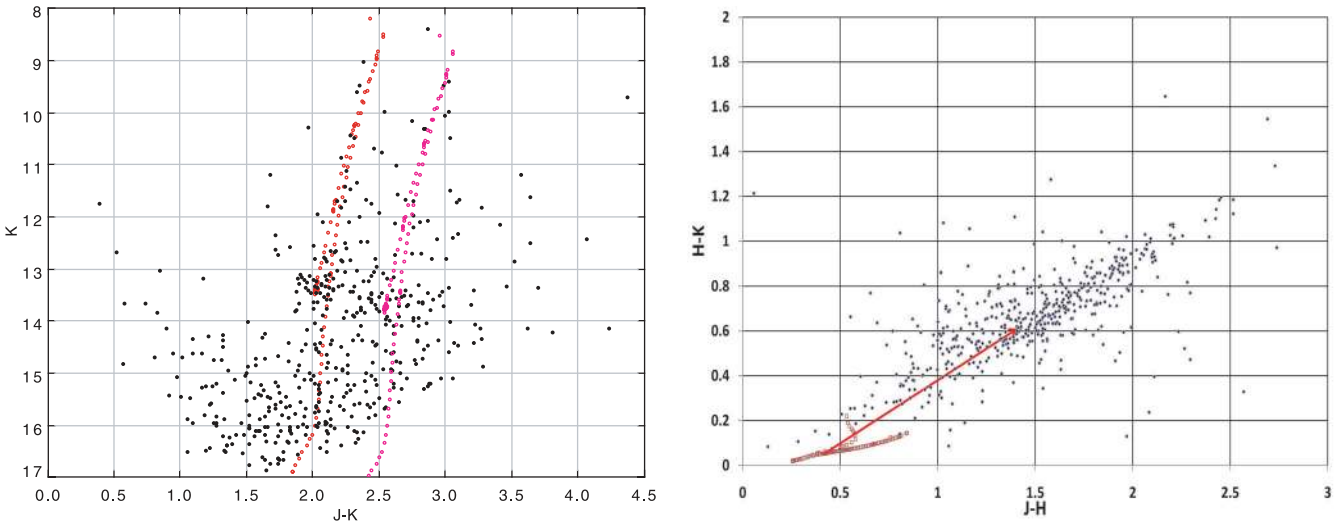

Figure 13. $r < 0.6$ arcmin region. Left-hand panel: examples of isochrones fitted by eye to clumps in the cluster. The black points show the CMDs for the whole cluster. Red points: fitting the HB clump, fit 6 in Table 9; magenta points: same isochrone but with $Av = 12$. Right-hand panel: $J-H$, $H-K$ diagram, with a reddening vector (red line) of 9.0 mag from the HB clump in isochrone 10^{10} yr, [Fe/H] $= 0.0024$ dex (maroon points).

Table 8. Derived reddening and distance modulus for Mercer 5 based on various assumptions about the cluster metallicity and the nature of the clump of stars in the CMD, based on empirical comparisons with known globular clusters (see text).

Fe/H (dex)	$M_{K,0}$	$(J-K)_0$	$(H-K)_0$	A_V (1)	A_V (2)	A_K (1)	$(m-M)_0$ (1)	$(m-M)_0$ (2)
−0.9 (c)	−1.36	0.47	0.028	9.0	9.1	0.99	13.69	13.68
−0.9 (b)	−1.44	0.59	0.088	8.3	8.1	0.91	13.85	13.87
−1.3 (c)	–	–	–	–	–	–	–	–
−1.3 (b)	−1.83	0.58	0.105	8.4	7.8	0.92	14.23	14.29

Table 9. Results of by-eye fitting of isochrones to the northern half of $r < 0.6$ arcmin region cluster CMD. Columns 3 and 4 indicate fits interpreting observed clump as an RGB bump and an HB clump, respectively.

Age (fit #)	[Fe/H] (dex)	$A_V(K, J-K$ fit)		$A_V(K, H-K$ fit)		$(m-M)_0$	
		RGBb	HBc	RGBb	HBc	RGBb	HBc
2×10^9 (1)	−1.3	8.7	9.2	8.5	8.7	14.9	13.9
4×10^9 (2)	−1.3	8.6	9.1	8.5	8.7	14.6	13.8
1×10^{10} (3)	−1.3	8.6	9.3	8.5	8.8	14.2	13.5
2×10^9 (4)	−0.9	8.5	9.0	8.5	8.7	14.6	14.0
4×10^9 (5)	−0.9	8.5	8.9	8.5	8.6	14.3	13.9
1×10^{10} (6)	−0.9	8.4	9.0	8.4	8.7	13.9	13.7
1×10^{10} (7)	0.0 (solar)	7.9	8.1	8.1	8.2	13.4	14.0

highly sensitive to the precise law. Results of the by-eye fits, either to the HB clump or to the RGB bump, are summarized in Table 9, with a solar metallicity result given also for comparison.

The main effect of increasing age is to make the K-band magnitude of both the RGB bump and the HB clump fainter, with very little effect on colour (hence A_V estimate). Assuming different metallicity also has only a small influence on colour, except for the solar metallicity comparison. With no independent information on the age of the cluster, we adopt a nominal value of 1×10^{10} yr, but comment further in Section 5.4. The $J-H$, $H-K$ CMD in Fig. 13 also shows a reddening vector of 8.96 mag originating at the location of the HB clump, for isochrone fit 6 in Table 9. The cluster overdensity locus in this diagram compared to the background annulus is fully consistent with expectations of a differentially reddened globular cluster in which the dominant population detected comprises giants and HB clump stars.

5.4 Adopted distance and reddening

To determine finally a distance and reddening value, we need to decide whether the dominant clump observed is an RGB bump or an HB clump. Examining in detail the K, $J-K$ CMDs of the clusters as shown in Ferraro et al. (2000), Cho & Lee (2002), Kim et al. (2006) and Valenti et al. (2007), in general for [Fe/H] ≥ -0.9 dex the HB clump is by far the strongest clump feature. For the range $-1.5 <$ [Fe/H] < -0.9 dex the RGB bump becomes slightly stronger relatively, with the HB becoming more extended. For clusters with [Fe/H] < -1.5 dex there is typically not a strong clump at all. Therefore, at the metallicity [Fe/H] ~ -1.3 dex we derive from the spectroscopy, an RGB bump is a more likely interpretation. Globular clusters around this range ([Fe/H] values given in parentheses) include M3 (−1.34), NGC 6355 (−1.42), NGC 6401 (−1.37) and NGC 6642 (−1.20). Taking M3 as a prime example because it is nearby, has high-S/N data and low reddening, Kim et al. (2006) show that it has an RGB bump at $M_{K,0} \sim -1.8$. This agrees very well with the isochrone value of −1.79 mag used in Table 9 for [Fe/H] = −1.3 dex and age 1×10^{10} yr to deduce the distance modulus, and also the empirical value of −1.83 mag from the Valenti et al. (2007) formulae. The empirical $(J-K)_0$ colour also compares quite well with the isochrone (0.58 and 0.55 mag, respectively), although the equivalent $(H-K)_0$ values of 0.105 and 0.065 mag lead to substantially different reddening estimates because of the short baseline.

There are two reasons to question the RGB bump interpretation. First, the clump seen in Mercer 5 is probably more dominant than the RGB bump seen empirically in clusters; secondly, if the 'clump' is an RGB bump, where is the horizontal branch in Mercer 5? There is a distinct gap in the CMD below and to the left of the clump.

If [Fe/H] ~ -0.9 dex we would interpret the clump as red HB stars, because both empirically and in the isochrones this is by far the most dominant feature of a globular cluster near-IR CMD. Using arguments similar to those above, we could again derive consistent empirical and isochrone solutions but the distance modulus would be ∼0.6 mag smaller (i.e. closer) and the extinction ∼0.6–0.7 mag higher than if we are seeing an RGB bump. It should also be noted that even at [Fe/H] ≤ -1.3 dex the isochrones still predict the strongest clumping in a K, $J-K$ or K, $H-K$ CMD should be the HB clump, but in the empirical diagrams cited above the HB is usually much more extended in K magnitude, giving little impression of a clump.

We are therefore faced with a dilemma: adopt the formal value of metallicity as indicated from the limited spectroscopy of a few stars, or use a metallicity that is at the upper limit allowed by the spectroscopy but then makes a stronger clump more likely and avoids the question of 'where are the HB stars?' Our preference at this stage, because of the dominance of the clump over any other feature, is the HB clump interpretation, adopting [Fe/H] $= -0.9$ dex $\Rightarrow (m-M)_0 = 13.7 \pm 0.2$, distance $= 5.5 \pm 0.5$ kpc and $A_V = 9.0 \pm 0.3$ for the least reddened part of the cluster. The alternative, not entirely ruled out, based on a prominent RGB bump, implies [Fe/H] $= -1.3 \Rightarrow (m-M)_0 = 14.2 \pm 0.2$, distance $= 6.8 \pm 0.5$ kpc and $A_V = 8.6 \pm 0.3$ for the least reddened part of the cluster.

5.5 Simulation of cluster using empirical data

We tried one more test of our HB clump interpretation. NGC 6539, with [Fe/H] ~ -0.8 dex, is a globular cluster with a prominent HB clump. Although it has slightly higher metallicity than we would

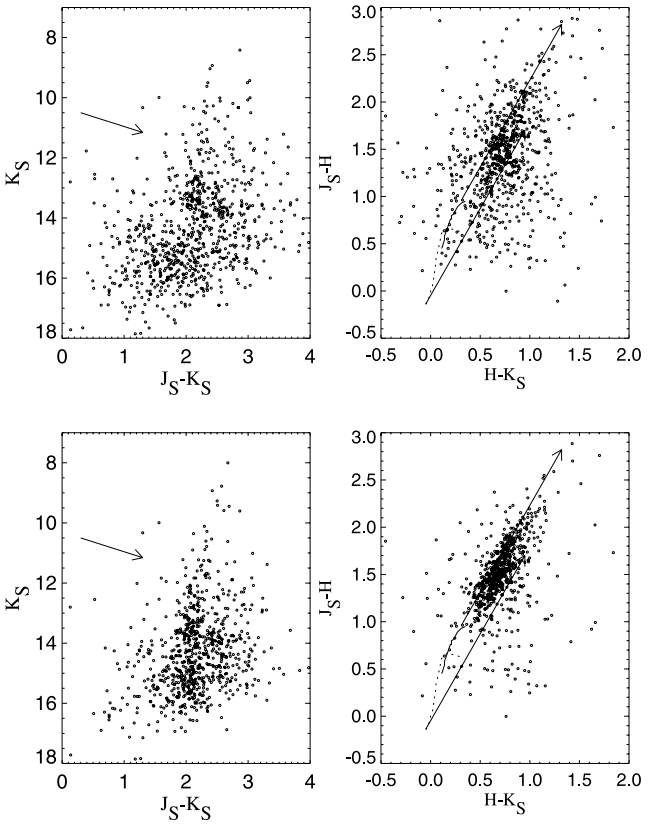

Figure 14. Top: SofI short-exposure observations of Mercer 5. Bottom: the same diagrams, but containing simulated, differentially reddened and distance-shifted data based on observations of NGC 6539 (see text for details).

want to adopt for Mercer 5, it has a very clear CMD with minimal foreground and background field star contamination. We used observational data of this cluster from Valenti et al. (2004) to investigate the effect of differential reddening. The cluster was divided into four quadrants, three of which were reddened independently by $E(J-K) = 1.0$, 1.4 and 1.8 mag. Additional, magnitude-dependent but otherwise random errors of magnitude and colour were added to each star, with limiting magnitudes set to be similar to those of the SofI short-exposure observations of Mercer 5. The results for the three quadrants were combined into a CMD and a CCD, with stars added from an appropriately sized background annulus around Mercer 5. The results are shown in Fig. 14 (bottom), along with similar diagrams from Mercer 5 itself (top). Arrows in the $J-H, H-K$ diagrams show vectors covering the reddening locus of a fiducial line (dotted, in the bottom left of the figure) of luminosity class III star from Koorneef (1983). While to some extent tailored to match our interpretation of Mercer 5, the simulations nevertheless still look remarkably like the observations in both diagrams and we believe that this further supports the HB clump interpretation in evaluating the distance and reddening to Mercer 5.

5.6 Other derived properties

5.6.1 Absolute size and luminosity

Integrating all the flux for an aperture of radius 0.6 arcmin, and correcting for the average background flux of sky + stars, gives an apparent magnitude $m_K = 6.6 \pm 0.3$. Fig. 3 shows the integrated flux diagram out to a radius of 2 arcmin, but at such large apertures the value chosen for the background star-plus-sky flux impacts significantly on the cluster total brightness and extent (as seen from the range of tidal radii deduced). For any backgrounds >4160 count pixel^{-1}, the integrated flux continues growing until the edge of the 2.5 arcmin radius field used for this measurement. At this background level the aperture photometry reaches a maximum at $r =$ 60 arcsec, with $m_K \sim 5.3$. Absolute magnitudes using the distance and A_V options derived above are listed in Table 10.

Table 10. Summary of derived parameters.

Parameter	Clump = RGB, [Fe/H] = −1.3 dex	Clump = HB, [Fe/H] = −0.9 dex
A_V (mag)	8.55	8.96
$(m-M)_0$	14.2	13.7
d (kpc)	6.8	5.5
$r_{0.5}$ (pc)	0.56	0.47
$m_{K,0}$ (mag)	5.7	5.5
$M_{K,0}$ (mag)	−8.5	−8.1
$M_{V,0}$ (mag)	−6.1	−5.5
L_x (erg s^{-1})	1.5×10^{33}	1.0×10^{33}

The cluster was not well fitted by a King profile because of poor determination of the tidal radius and the dependency on the sampling radius, so we have calculated the cluster scale based on the nominal half-light radius, also given in the summary table.

5.6.2 X-ray source XMMU J182319.8−134011

We searched the 2XMM data base (Watson et al. 2009) for X-ray sources coincident with Mercer 5. One is found at RA = $18^{\rm d}23^{\rm m}19\overset{\rm s}{.}73$, Dec. = $-13^\circ40'9\overset{''}{.}2$, with a positional uncertainty of 1.1 arcsec. We have made a visual inspection of the source, and have verified that the source is in a clean region on all the *XMM* EPIC detectors. The flux of the X-ray source is 2.8×10^{-13} erg cm^{-2} s^{-1} from 0.2 to 12 keV, which corresponds to a luminosity of 1.5×10^{33} erg s^{-1} for a distance of 6.8 kpc or 1.0×10^{33} erg s^{-1} for 5.5 kpc.

We can then compute the probability that the X-ray source association is because of chance superposition. There is only one other source above 10^{-13} erg s^{-1} cm^{-2} within 8 arcmin of the cluster centre. Assuming that we would have considered any match within the half-light radius of 17 arcsec to have been interesting, the chance superposition probability is thus about 1 in 800. The probability of finding a source within 4 arcsec of the cluster centre is thus only about 7×10^{-5}, indicating a high probability of association with the cluster. We note that it is surprising to find such a bright X-ray source in such a low-luminosity cluster, and thus that this source merits future follow-up to determine whether it might have been formed earlier in the lifetime of the cluster when it was much more massive (see e.g. Fregeau 2008 for a discussion of how cluster evolution should affect the number of X-ray sources).

6 DISCUSSION

Throughout this paper, we have tended to work on the assumption that Mercer 5 is a globular cluster. In Table 10 we summarize the parameters derived above and in the current section based on this assumption, for both alternative explanations for the stellar clump in the CMDs.

This approach was based on the combination of its appearance (allowing for possible differential reddening causing the apparent east–west elongation) and the results of the metallicity determination of the stars for which we have spectroscopy. But how confident can we be of this classification?

Determining the distance was made difficult because even off-cluster reference area CMDs showed a similar (but weaker) clump of stars in the region of the cluster clump (see Figs 1, 4 and 5). This could be evidence (see Section 5.1) that the cluster extends further than 1 arcmin in radius, or they might be RGB and/or HB clump stars at a similar distance to the cluster. Cabrera-Lavers et al. (2008) use UKIDSS data to analyse Galactic structure, employing red clump star counts as indicators, and confirm the existence of a Galactic bar extending out to a longitude of 28°. Adopting their position angle of 42°.4, in the direction of Mercer 5, the Galactic bar would be at a distance of 6.2 kpc for a Galactic Centre distance of 8 kpc. Robin (private communication) also provided an example $K, J-K$ CMD from a Besançon development model that includes a Galactic bar. No features were visible in this model that would readily explain the clump features of our CMDs.

Globular clusters will slowly be disrupted by dynamical shocks suffered during successive passages through the Galactic plane (e.g. Ostriker, Spitzer and Chevalier 1972). If Mercer 5 is a globular cluster in the process of being tidally destroyed by the Galaxy, one would expect that its absolute magnitude lies within the range of known Galactic globular clusters but probably on the tail towards low luminosity. Adopting the $(V-K)_0$ − metallicity relation as given in Frogel, Persson & Cohen (1980) allows the integrated visual magnitude of the cluster to be calculated as $M_{V,0} = -5.4$ mag for our preferred distance. This is well within the low-luminosity tail of the Galactic globular cluster luminosity function (e.g. Di Criscienzo et al. 2006, their fig. 3). The persistence of the red clump well outside the easily defined area of the cluster is at least consistent with such an interpretation, although it must be regarded as speculative without further evidence.

Is an alternative explanation of Mercer 5, as an old open cluster, viable? Such clusters are scarce in number, tend to be concentrated towards the Galactic anticentre, and are almost totally absent inside 7.5 kpc from the Galactic Centre (Janes & Phelps 1994; Froebrich et al. 2010). Janes & Phelps (1994) argue that this effect is real and not caused by observational bias, because they would have found many within that radius had they been present: no such limitation is found for younger clusters. It is generally thought (first pointed out by Spitzer 1958 and summarized by Friel 1995) that this absence is because frequent encounters with large gas clouds within the inner regions of the Galaxy effectively destroy the clusters, implying a smaller likelihood of Mercer 5 being an old open cluster candidate. Nevertheless the interpretation of Mercer 5 as an old open cluster cannot be ruled out completely, as was recently shown by Davies at al. (2011) for GLIMPSE-C01. Based on high-resolution near-IR spectroscopy, they concluded that GLIMPSE-C01 is most probably old open cluster instead of globular.

New surveys such as those done with 2MASS, GLIMPSE and UKIDSS have so far found a very small number of new globular cluster candidates well within this 7.5 kpc region, but statistical interpretation of the results awaits, at least, a detailed simulation to quantify the detection limits of the surveys for such clusters.

Investigating the *Spitzer* data for mid-IR excess emission provides no compelling evidence for recent star formation. In the case of a young open cluster a main sequence including some high-mass stars would be expected, but with no clumps in the CMD, completely inconsistent with our observations.

The K-band spectra of five likely cluster giants are consistent with those of RGB stars, although they tend to indicate lower metallicity than implied by the existence of a dominant red HB clump.

7 CONCLUSIONS

Detailed investigation of one of the clusters discovered in the *Spitzer* GLIMPSE survey, Mercer 5, highlights the challenge of producing unique determinations of cluster properties in crowded, very low galactic latitude fields. The most self-consistent interpretation of Mercer 5 is as a Galactic globular cluster. Although we are unable to distinguish unequivocally between an RGB bump or an HB clump interpretation for the IR CMD of such a cluster, we have presented several arguments that lead us to prefer the HB clump interpretation. In this case Mercer 5 is at ∼5.5 kpc distance: on either model the least reddened, northern part of the cluster suffers ∼9 mag of visual extinction. It has a small dust cloud located coincidentally in front of the southern half the cluster, which suffers up to a further ∼4 mag of visual extinction.

ACKNOWLEDGMENTS

The SofI data were obtained under the ESO programme ID 077.D-0089(A). JB is supported by FONDECYT No. 1080086 and by the Ministry for the Economy, Development and Tourism's Programa Inicativa Cientìfica Milenio through grant P07-021-F, awarded to The Milky Way Millennium Nucleus, and RK acknowledges support from DIPUV/CID No. 3/2006, 'Centro de astrofìsica de Valparaìso. RdG acknowledges support from the National Natural Science Foundation of China (grants 11043006 and 11073001). We thank Annie Robin for providing the extinction curve in the direction of Mercer 5 derived from the Marshall et al. (2006) paper and for running for us the Besançon development model that includes the Galactic bar.

REFERENCES

Aguirre J. E. et al., 2011, ApJS, 192, 4
Barbuy B., Bica E., Ortolani S., 1998, A&A, 333, 117
Bastian N., Konstantopoulos I., Smith L. J., Trancho G., Westmoquette M. S., Galagher J. S., 2007, MNRAS, 379, 1333
Benjamin R. A. et al., 2003, PASP, 115, 953
Bonatto C., Bica E., Ortolani S., Barbuy B., 2007, MNRAS, 381, 45
Borissova J., Pessev P., Ivanov V. D., Saviane I., Kurter R., Ivanov G. R., 2003, A&A, 411, 83
Borissova J., Ivanov V. D., Minniti D., Geisler D., Stephens A. W., 2005, A&A, 435, 95
Borissova J., Ivanov V. D., Minniti D., Geisler D., 2006, A&A, 455, 923
Burningham B. et al., 2010, MNRAS, 406, 1885
Cabrera-Lavers A., González-Fernández C., Garzón F., Hammersley P. L., López-Corredoira M., 2008, A&A, 491, 781
Cardelli J. A., Clayton G. C., Mathis J., 1989, ApJ, 345, 245
Carraro G., 2005, ApJ, 621, L61
Cho D-W., Lee S-G., 2002, AJ, 124, 977
Cohen J. G., 2006, ApJ, 653, L21
Davies B., Bastian N., Gieles M., Seth A. C., Mengel S., Konstantopoulos I. S., 2011, MNRAS, 411, 1386
Davis L. E., 1994, iraf.noao.edu/iraf/ftp/iraf/docs/daorefman.ps.Z.
Di Criscienzo M., Caputo F., Marconi M., Musella I., 2006, MNRAS, 365, 1357
Dutra C. M., Bica E., 2001, A&A, 376, 434
Ferraro F. R., Montegriffo P., Origlia L., Fusi Pecci F., 2000, AJ, 119, 1282
Ferraro F. R., Valenti E., Origlia L., 2006, ApJ, 649, 243
Fitzpatrick E. L., Massa D., 2009, ApJ, 699, 1209

Fregeau J. M., 2008, ApJ, 673, L25
Friel E. D., 1995, ARA&A, 33, 381
Froebrich D., Meusinger H., Scholz A., 2007a, MNRAS, 377, L54
Froebrich D., Scholz A., Raftery C. L., 2007b, MNRAS, 374, 399
Froebrich D., Schmeja S., Samuel D., Lucas P. W., 2010, MNRAS, 408, 1281
Frogel J. A., Persson S. E., Matthews K., Aaronson M., 1978, ApJ, 220, 75
Frogel J. A., Persson S. E., Cohen J. G., 1980, ApJ, 240, 785
Frogel J. A., Stephens A., Ramirez S., DePoy D., 2001, AJ, 122, 1896
Hambly N. C. et al., 2008, MNRAS, 384, 637
Harris W. E., 1996, AJ, 112, 1487
He L., Whittet D. C. B., Kilkenny D., Spencer Jones J. H., 1995, ApJS, 101, 335
Hurt R. L., Jarrett T. H., Kirkpatrick J. D., Cutri R. M., Schneider S. E., Skrutskie M., van Driel W., 2000, AJ, 120, 1876
Ivanov V. D., Borissova J., Pessev P., Ivanov G. R., Kurtev R., 2002, A&A, 394, L1
Indebetouw R. et al., 2005, ApJ, 619, 931
Ivanov V. D., Borissova J., Bresolin F., Pessev P., 2005a, A&A, 435, 107
Ivanov V. D., Kurtev R., Borissova J., 2005b, A&A, 442, 195
Ivanov V. D., Messineo M., Zhu Q., Figer D., Borissova J., Kurtev R., Ivanov G. R., 2010, in de Grijs R., Lépine J. R. D., eds, Proc. IAU Symp. 266, Star Clusters: Basic Galactic Blocks Throughout Time and Space. Cambridge Univ. Press, Cambridge, p. 203
Janes K. A., Phelps R. L., 1994, AJ, 108, 1773
Kim J.-W. et al., 2006, A&A, 459, 499
King I. R., 1966, AJ, 71, 64
Koorneef J., 1983, A&A, 128, 84
Kurtev R., Borissova J., Georgiev L., Ortolani S., Ivanov V. D., 2007, A&A, 475, 209
Kurtev R., Ivanov V. D., Borissova J., Ortolani S., 2008, A&A, 489, 583
Lawrence A. et al., 2007, MNRAS, 379, 1599
Lucas P. W. et al., 2008, MNRAS, 391, 136
Lucas P. W. et al., 2009, Proc. 'UKIRT at 30′ Workshop', in press
Maiolino R., Rieke G. H., Rieke M. J., 1996, ApJ, 111, 537
Marigo P., Girardi L., Bressan A., Groenewegen M. A. T., Silva L., Granato G. L., 2008, A&A, 482, 883
Marshall D. J., Robin A. C., Reylé C., Schultheis M., Picaud S., 2006, A&A, 453, 635
Mercer E. P. et al., 2005, ApJ, 635, 560
Messineo M., Davies B., Ivanov V. D., Figer D., Schuller F., Habing H., Menten K., Petr-Gotzens M., 2009, ApJ, 697, 701
Minniti D. et al., 2010, New Astron., 15, 433
Minniti D. et al., 2011, A&A, 527, 81
Moorwood A., Cuby J. G., Lidman C., 1998, The Messenger, 91, 9
Ortolani S., Bica E., Barbuy B., 2000, A&A, 361, 57
Ortolani S., Bonatto C., Bica E., Barbuy B., 2009, AJ, 138, 889
Ortolani S., Barbuy B., Bica E., 2010, in de Grijs R., Lepine J. R. D., eds, Proc. IAU Symp. 266, Star Clusters: Basic Galactic Building Blocks. Cambridge Univ. Press, Cambridge, p. 97
Ostriker J. P., Spitzer L., Chevalier R. A., 1972, ApJ, 176, L51
Pfleiderer J., Weinberger R., Mross R., 1977, Star Cluster Symp. Vol. 5. Eotvos University, Budapest, p. 39
Robin A. C., Reylé C., Derrière S., Picaud S., 2003, A&A, 409, 523
Rieke G. H., Lebofsky M., 1985, ApJ, 288, 618
Spitzer L., 1958, ApJ, 127, 17
Stead J. J., Hoare M. G., 2009, MNRAS, 400, 731
Stephens A. W., Frogel J. A., 2004, AJ, 127, 925
Stetson P., Davis L. E., Crabtree D. R., 1990, in Jocoby G. H., ed., ASP Conf. Ser. Vol. 8, CCDs in Astronomy. Astron. Soc. Pac., San Francisco, p. 289
Stetson P., 1996, User's Manual for DAOPHOT II. Dominion Astrophysical Observatory, Victoria
Strader J., Kobulnicky H. A., 2008, AJ, 136, 2102
Valenti E., Ferraro F. R., Origlia L., 2004, MNRAS, 354, 815
Valenti E., Origlia L., Ferraro F. R., 2005, MNRAS, 361, 272
Valenti E., Ferraro F. R., Origlia L., 2007, AJ, 133, 287
Valenti E., Ferraro F. R., Origlia L., 2010, MNRAS, 402, 1729
Watson M. G. et al., 2009, A&A, 493, 339

This paper has been typeset from a MS Word file prepared by the author.